Quasi-laminar stability and sensitivity analyses for turbulent flows: Prediction of low-frequency unsteadiness and passive control

Clément Mettot, Denis Sipp, and Hervé Bézard

Citation: Physics of Fluids (1994-present) **26**, 045112 (2014); doi: 10.1063/1.4872225
View online: http://dx.doi.org/10.1063/1.4872225
View Table of Contents: http://scitation.aip.org/content/aip/journal/pof2/26/4?ver=pdfcov
Published by the AIP Publishing

PHYSICS OF FLUIDS **26**, 045112 (2014)

Quasi-laminar stability and sensitivity analyses for turbulent flows: Prediction of low-frequency unsteadiness and passive control

Clément Mettot, Denis Sipp, and Hervé Bézard
ONERA The French Aerospace Lab, 8 rue des Vertugadins, 92190 Meudon, France

(Received 10 October 2013; accepted 10 April 2014; published online 28 April 2014)

This article presents a quasi-laminar stability approach to identify in high-Reynolds number flows the dominant low-frequencies and to design passive control means to shift these frequencies. The approach is based on a global linear stability analysis of mean-flows, which correspond to the time-average of the unsteady flows. Contrary to the previous work by Meliga *et al.* ["Sensitivity of 2-D turbulent flow past a D-shaped cylinder using global stability," Phys. Fluids **24**, 061701 (2012)], we use the linearized Navier-Stokes equations based solely on the molecular viscosity (leaving aside any turbulence model and any eddy viscosity) to extract the least stable direct and adjoint global modes of the flow. Then, we compute the frequency sensitivity maps of these modes, so as to predict before hand where a small control cylinder optimally shifts the frequency of the flow. In the case of the D-shaped cylinder studied by Parezanović and Cadot [J. Fluid Mech. **693**, 115 (2012)], we show that the present approach well captures the frequency of the flow and recovers accurately the frequency control maps obtained experimentally. The results are close to those already obtained by Meliga *et al.*, who used a more complex approach in which turbulence models played a central role. The present approach is simpler and may be applied to a broader range of flows since it is tractable as soon as mean-flows — which can be obtained either numerically from simulations (Direct Numerical Simulation (DNS), Large Eddy Simulation (LES), unsteady Reynolds-Averaged-Navier-Stokes (RANS), steady RANS) or from experimental measurements (Particle Image Velocimetry - PIV) — are available. We also discuss how the influence of the control cylinder on the mean-flow may be more accurately predicted by determining an eddy-viscosity from numerical simulations or experimental measurements. From a technical point of view, we finally show how an existing compressible numerical simulation code may be used in a black-box manner to extract the global modes and sensitivity maps. © *2014 AIP Publishing LLC*. [http://dx.doi.org/10.1063/1.4872225]

I. INTRODUCTION

Turbulent flows are frequently encountered in applications and may exhibit strong low frequency unsteadiness. The oscillating behavior of the flow may lead to undesirable features such as structural vibrations or load fluctuations. For such applications, control methods may aim at shifting the associated frequency so as to prevent structural resonance for example. These methods generally require the understanding of the inherent mechanisms responsible for flow unsteadiness. Following the reviews by Collis *et al.*,[1] Chomaz,[2] Kim and Bewley,[3] and Sipp *et al.*,[4] the present article explores the potential of flow control based on a linear description of the flow dynamics; the present article focuses on fully developed turbulent flows presenting low-frequency unsteadiness.

Stability and sensitivity analyzes have first been applied in the case of transitional flows, which are governed by the Navier-Stokes equations based on the molecular viscosity μ. An equilibrium point of the governing equations — a *base-flow* — is first determined and the dynamics of small-amplitude perturbations around such flows is then analyzed. The base-flow is unstable if there

exists an unstable eigen-mode of the linearized governing equations. Sensitivity of the eigenvalues with respect to base-flow modifications have been introduced to analyze the sensitive regions of the flow.[5–8] Passive control (by means of a control cylinder, for example) may then be studied by considering the sensitivity of the eigenvalue with respect to the introduction of a steady forcing. The experimental control map obtained by Strykowski and Sreenivasan[9] in the case of the cylinder flow could precisely be recovered for a Reynolds number within 46–100.[8]

The extension of linear stability and sensitivity analyzes to turbulent flows is the purpose of this paper. The theoretical basis for such an extension is given in Reynolds and Hussain,[10] in which the flow-field is represented as

$$\mathsf{w} = \overline{\mathsf{w}} + \widetilde{\mathsf{w}} + \mathsf{w}', \tag{1}$$

where $\overline{\mathsf{w}}$ is the time-averaged flow, $\widetilde{\mathsf{w}}$ is a low-frequency, large-scale, organized periodic wave, and w' corresponds to turbulent motions. The organized-wave $\widetilde{\mathsf{w}}(t)$ is extracted thanks to $\widetilde{\mathsf{w}}(t) = \langle \mathsf{w} \rangle(t) - \overline{\mathsf{w}}$, where $\langle \mathsf{w} \rangle(t)$ is a phase-average operator based on the fundamental period T of the low-frequency motions: $\langle \mathsf{w} \rangle(t) = \lim_{n\to\infty} \frac{\sum_{i=0}^{n-1} \mathsf{w}(t+iT)}{n}$. The time-averaged flow $\overline{\mathsf{w}}$ is governed by steady Navier-Stokes equations driven by Reynolds stresses stemming both from the organized wave $\overline{\widetilde{u}_i \widetilde{u}_j}$ and from the turbulent motions $\overline{u_i' u_j'}$ (Eq. (2.5) in Reynolds and Hussain[10]). Meanwhile, the dynamics of a (small amplitude) organized wave $\widetilde{\mathsf{w}}$ is governed by Navier-Stokes equations linearized around $\overline{\mathsf{w}}$, with an extra driving-term representing the oscillation of the Reynolds stresses $\widetilde{u_i' u_j'}$ induced by the passage of the organized wave $\widetilde{\mathsf{w}}$ (Eq. (2.6) in Reynolds and Hussain[10]). Note that without further assumption, these two equations are coupled (the time-averaged flow and the organized wave appear in both equations) and may not be solved separately. In the literature, there actually exist two types of stability analyzes for turbulent flows, depending on the type of time-averaged flow that is considered. The *base-flow approach* is concerned with stability of time-averaged flows $\overline{\mathsf{w}}$ solely driven by Reynolds stresses stemming from the turbulent motions $\overline{u_i' u_j'}$. This means that the corresponding flow-field only exhibits unsteadiness characterized by high-frequency, fine-scale turbulence w', and no low-frequency, large-scale organized waves $\widetilde{\mathsf{w}}$. In such a case, the time-averaged flow will be termed *base-flow* in the following. The equation governing this base-flow is then decoupled from the organized wave equation and the stability of the base-flow can therefore be assessed by analyzing the dynamics of small-amplitude organized waves superimposed on the base-flow. Particular attention will be paid to the amplification mechanisms. For example, if the base-flow is stable, then the phase-averaged flow $\langle \mathsf{w} \rangle$ will converge to the base-flow $\overline{\mathsf{w}}$; if not, an organized wave $\widetilde{\mathsf{w}}$ will grow and the phase-averaged flow $\langle \mathsf{w} \rangle$ moves away from the base-flow $\overline{\mathsf{w}}$. The *mean-flow approach* is concerned with the stability of time-averaged flows $\overline{\mathsf{w}}$ driven by stresses arising both from organized waves $\overline{\widetilde{u}_i \widetilde{u}_j}$ and from turbulent motions $\overline{u_i' u_j'}$. In this case, the time-averaged flow will be called a *mean-flow* in the following. As mentioned above, the equations governing the mean-flow and the organized wave are coupled in such cases: the results of the stability analysis need therefore to be interpreted in a particular way; it turns out (see below) that only the frequency of a nearly marginal eigen-mode exhibits physical insight and that its frequency usually matches the frequency of the organized wave in the true flow. We will now give some more details on the *base-flow* and *mean-flow* approaches.

A. Base-flow approach

To proceed with the base-flow approach, it is necessary to consider a turbulence model. In the following, the Reynolds-Averaged-Navier-Stokes equations closed with such a model will be termed RANS equations. These allow to obtain closed equations for both the base-flow $\overline{\mathsf{w}}$ and the organized wave $\widetilde{\mathsf{w}}$. For example, in the case of homogeneous incompressible equations, an eddy viscosity model based on the kinetic energy $\rho\langle k \rangle = \rho\langle u_i' u_i' \rangle/2$ and on the turbulent dissipation-rate $\rho\langle \epsilon \rangle = \mu\langle \partial_j u_i' \partial_j u_i' \rangle$ yields the following phase-averaged Reynolds stress tensor:

$$\rho\langle u_i' u_j' \rangle = \frac{2}{3}\rho\langle k \rangle \delta_{ij} - 2\frac{\rho C_\mu \langle k \rangle^2}{\langle \epsilon \rangle}\langle S_{ij} \rangle. \tag{2}$$

Here, $C_\mu = 0.09$, $S_{ij} = (\partial_i u_j + \partial_j u_i)/2$ is the symmetric velocity gradient tensor and δ_{ij} is the Kronecker symbol. Note that we used the Einstein-summation convention in the definitions of the kinetic energy and turbulent dissipation. For small-amplitude organized waves, Eq. (2) yields at the leading and at the next order

$$\rho\overline{u_i' u_j'} = \frac{2}{3}\rho\overline{k}\delta_{ij} - 2\overline{\mu_t}\overline{S}_{ij}, \tag{3}$$

$$\rho\widetilde{u_i' u_j'} = \frac{2}{3}\rho\widetilde{k}\delta_{ij} - 2\overline{\mu_t}\widetilde{S}_{ij} - 2\widetilde{\mu_t}\overline{S}_{ij}, \tag{4}$$

with $\overline{\mu_t} = \frac{\rho C_\mu \overline{k}^2}{\overline{\epsilon}}$ and $\widetilde{\mu_t} = \frac{2\rho C_\mu \overline{k}\widetilde{k}}{\overline{\epsilon}} - \frac{\rho C_\mu \overline{k}^2 \widetilde{\epsilon}}{\overline{\epsilon}^2}$. The equation governing the phase-averaged turbulent kinetic energy $\langle k \rangle$ (resp. the phase-averaged turbulent dissipation $\langle \epsilon \rangle$) then yields a nonlinear equation for $\overline{k}$ (resp. $\overline{\epsilon}$) and a linear-equation for $\widetilde{k}$ (resp. $\widetilde{\epsilon}$) if small-amplitude organized waves are considered. As a result, the base-flow corresponds to a steady solution of the RANS equations while the organized wave is governed by the unsteady linearized RANS equations. Such a study has been led in the case of transonic buffet over an airfoil by Crouch, Garbaruk, and Magidov[11] and on a transonic cavity flow by Mettot, Renac, and Sipp.[12] The amplification rate of the eigen-vector is a meaning-full quantity, that may be used as an objective to suppress organized waves in open-loop control strategies.[12] On the other hand, the frequency of the eigen-mode only matches the true low-frequency of the organized wave in the vicinity of the bifurcation threshold, where the amplification rate is nearly zero. For super-critical parameters, i.e., when the amplification rate of the global mode is of order 1, one has to take into account the frequency shift due to nonlinear interactions to accurately predict the true low-frequency of the organized wave. This frequency shift may be evaluated by computing the mean-flow and second harmonic components of the flow, which are strong components of the flow-field due to the finite amplitude of the organized wave.[13] Prerequisites for the base-flow approach to predict a relevant low-frequency of the flow are therefore:

- the existence of a turbulence model that captures the low-frequency large-scale flow dynamics; limitations of the unsteady RANS strategy have been highlighted by Shur *et al.*[14] and Spalart[15] in the case of the circular cylinder, for example;
- the existence of a fixed point to linearize about the dynamics;
- to remain close to the bifurcation threshold so that nonlinearities maintain the organized wave at small amplitudes (in order to keep the nonlinear frequency shift weak).

In some configurations, an approximation may be performed by choosing a frozen eddy-viscosity $\widetilde{\mu_t} = 0$, which means that neither the turbulence energy ($\widetilde{k} = 0$) nor its dissipation rate ($\widetilde{\epsilon} = 0$) is oscillated by the perturbation. In this case, the stability analysis is based on the linearized Navier-Stokes equations with a viscosity equal to the sum of the molecular-viscosity μ and the eddy-viscosity $\overline{\mu_t}$ of the base-flow. In the case of cavity flow, Mettot, Renac, and Sipp[12] showed that the eigenvalues of the frozen eddy-viscosity operator are close to those of the full linearized operator, while Juan and Jiménez[16] and Cossu, Pujals, and Depardon[17] showed that this simplified approach successfully predicted strong transient growth mechanisms associated to very large scale perturbations in channel and boundary layer flows. In the case of the buffeting flow, Crouch, Garbaruk, and Magidov[11] showed that a frozen eddy-viscosity approach was not capable of capturing the unstable global modes, all the global modes remaining stable as the Mach number or the angle of attack was increased.

B. Mean-flow approach

If there is a difficulty with one of the prerequisites listed above, then the mean-flow approach may be followed, since *mean-flows* may straightforwardly be obtained in any experiment or numerical simulation by time-averaging. In the literature, stability analyzes around *mean-flows* were generally based on the linearization of either the Euler or the Navier-Stokes equations (at high Reynolds numbers, these linear operators are close). The question of the relevance of eigenvalues/eigenvectors associated to such linearized operators is therefore raised. Reynolds and Hussain[10] argued that

such approaches implicitly assume that the turbulence affects the wave only indirectly, through the modified time-averaged flow — we consider a mean-flow and not a base-flow — and not directly, through its stresses — we assume $\widetilde{u_i' u_j'} = 0$. Past studies have shown that they were actually efficient means to predict the frequency of organized waves in turbulent flows. Piot *et al.*,[18] Suzuki and Colonius,[19] and Gudmundsson and Colonius[20] showed that either linearized Euler or linearized Navier-Stokes equations around the *mean-flow* successfully exhibited the frequency of a compressible subsonic or supersonic jet. Same conclusions were obtained by Mattingly and Criminale,[21] Triantafyllou, Triantafyllou, and Chryssostomidis,[22] Pier,[23] and Thiria and Wesfreid[24] in the case of flat-plate, airfoil, and cylinder wakes, by Hammond and Redekopp[25] in mixing layers, and by Barkley[26] with incompressible linearized Navier-Stokes equations (global approach) in cylinder wakes. At much higher Reynolds numbers, Juniper[27] showed that stability analyzes based on Orr-Sommerfeld equations were successful in predicting the unsteady frequencies in a single stream swirling fuel injector and in a lean premixed gas turbine injector with five swirling streams. In these studies, only the frequency of the modes is relevant. For cylinder flow, for example, Barkley[26] showed, thanks to a global linear stability study, that the mean-flow exhibits a global mode displaying the true-frequency of the flow but that the amplification rate was marginally stable for all Reynolds numbers in the range $Re = 46 - 180$. There actually exists a theoretical explanation to these observations, which is valid when the *mean-flow* is close to a *base-flow*. In this case, Sipp and Lebedev[13] showed that the *mean-flow* exhibits a nearly marginally stable eigen-mode with a frequency that matches the frequency of the true flow, if the mean-flow harmonic is much stronger than the second harmonic. These studies are reminiscent of early works by Malkus,[28] who conjectured that developed turbulent flows should be stable. Obviously, it seems that the *mean-flow approach* is valid for a large variety of flows. A hypothesis could be that all flows that are driven by Kelvin-Helmholtz like instabilities (jets, shear-layers, wakes) could be analyzed with this approach. In the following, the mean-flow approach will be termed *quasi-laminar approach*, as we use linearized Navier-Stokes equations (and not Euler equations).

C. Approach by Meliga, Pujals, and Serre and objective of the present paper

Meliga, Pujals, and Serre[29] actually did a study which mixes the base-flow and the mean-flow approaches. Considering the case of a two-dimensional (2D) D-shaped cylinder at a moderately high Reynolds number of $Re = 13\,000$ (a flow driven by Kelvin-Helmholtz like instabilities), they have computed a *mean-flow* (as required by the mean-flow approach) by time-averaging unsteady 2D RANS simulations, showed that the full-linearized RANS equations (as required by the base-flow approach) exhibit a nearly marginal global mode, whose frequency is close to the natural one (as expected by the mean-flow approach). They then studied the effect on the flow frequency of the introduction of a small control cylinder in the flow by using a sensitivity analysis and found that the frequency control map was in close agreement with the experimental study of Parezanović and Cadot.[30] Their results suggest that a sensitivity analysis may be a powerful method to design open-loop control strategies to shift the low-frequency of a turbulent flow. We believe, and it is the purpose of this article, that a simpler approach, i.e., a pure *mean-flow approach*, which is still based on the *mean-flow*, but with linearized Navier-Stokes equations based on the molecular viscosity, could yield similar results. This would be an important step since:

- the *mean-flow approach* does not rely on a turbulence model; it is therefore much simpler — linearization of turbulence equations is painful, error-prone, and induces lots of numerical difficulties — more general — even unsteady flows that may not be reproduced by unsteady 2D RANS simulations may be analyzed — and may even be more accurate — because *mean-flows* should be more precisely determined if more accurate methods than unsteady 2D RANS simulations were used. In so far, application of the *mean-flow approach* should path the way to applications of stability and sensitivity analyzes to more industrial configurations.
- It yields better physical insight to understand why a control cylinder at high Reynolds numbers may be efficient to shift the low-frequency of a turbulent flow.

To make this point, we propose to revisit the D-shaped cylinder configuration with this simplified approach. An accurate *mean-flow* will be determined by time-averaging three-dimensional (3D) numerical simulations. This *mean-flow* should be more accurate than the one considered in Meliga, Pujals, and Serre[29] since 3D unsteady simulations are closer to reality than 2D unsteady simulations.[14,15,31] The quality of the quasi-laminar predictions will be assessed by comparison of the results with those of Parezanović and Cadot[30] and Meliga, Pujals, and Serre.[29] Note finally that this article also aims at presenting a sound and robust numerical approach for the extraction of the Jacobian and Hessian-related quantities within a discretize-then-linearize approach. The procedure is solely based on discrete residual evaluations and allows the use of a standard numerical code in a black-box manner. More details are given in Mettot, Renac, and Sipp.[12] We believe that the present numerical approach is well suited for the application of stability and sensitivity analyzes in industrial applications.

The paper is organized as follows. We present in Sec. II the theoretical background to perform the quasi-laminar stability and sensitivity analyzes. The numerical procedure used to perform these analyzes is detailed in Sec. III and we will show how a numerical code can be used to extract eigenmodes and sensitivities around mean-flows in the case of compressible Navier-Stokes equations. In Sec. IV, the unsteady 3D dynamics of the D-shaped cylinder is presented and a two-dimensional mean-flow is computed from the unsteady data set. The linear stability of the mean-flow with a molecular viscosity μ is probed in Sec. V and it is shown that the unsteady dynamics of the flow is caused by the existence of a slightly unstable mode. The sensitivity analysis is performed in Sec. VI, and the impact of a small steady cylinder onto the unstable mode's frequency is computed. We will analyze how the eigenvalues and frequency control maps associated to the quasi-laminar approach compare with those of Parezanović and Cadot[30] and Meliga, Pujals, and Serre.[29] Improvements for the evaluation of the effect of the control cylinder on the mean-flow will be discussed in Sec. VII. A brief summary and some concluding remarks will be given in Sec. VIII.

II. QUASI-LAMINAR STABILITY AND SENSITIVITY ANALYZES OF MEAN-FLOWS

We consider a turbulent flow in a fixed configuration. In this case, the ensemble average of the flow-field is steady and we may define the mean-flow as

$$\overline{\mathsf{w}}(\mathsf{x}) = \lim_{T\to\infty} \frac{1}{T} \int_0^T \mathsf{w}(\mathsf{x}, t)\, dt. \tag{5}$$

In the case of a configuration which is invariant in some direction, the mean-flow $\overline{\mathsf{w}}(\mathsf{x})$ does not depend on the coordinate linked to this direction, so that the mean-flow may be obtained by averaging both in time and along the invariant direction.

We now superimpose small amplitude organized waves $\widetilde{\mathsf{w}}(\mathsf{x}, t)$ onto the mean-flow $\overline{\mathsf{w}}(\mathsf{x})$ and consider the Navier-Stokes equations linearized around $\overline{\mathsf{w}}$ with only the molecular dynamic viscosity μ (with neither a turbulence model nor an eddy viscosity $\overline{\mu}_t$). This approximation renders the whole procedure very general, since the mean-flow $\overline{\mathsf{w}}$ can easily be obtained from experimental or Direct Numerical Simulation (DNS). Considering normal modes of the form $\widetilde{\mathsf{w}} = \hat{\mathsf{w}} e^{\lambda t}$, where $\lambda = \sigma + i\omega$ describes the amplification rate σ and frequency ω of the perturbation, the linearized Navier-Stokes equations reduce to an eigenvalue problem

$$\mathsf{J}\hat{\mathsf{w}} = \lambda \hat{\mathsf{w}}. \tag{6}$$

In this equation, J designates the linearized Navier-Stokes operator with viscosity μ. Experience has shown that there generally exists an eigen-mode that displays weak amplification rate and a frequency that is close to the dominant frequency of the flow in the experiment or the DNS. Hence, the present stability analysis should allow the identification of the dominant frequencies of a flow by investigating the mean-flow stability.

We will now describe how to determine sensitive regions that lead to strongest shift of the frequency of the flow. For this, we derive the sensitivity gradient of the eigenvalue to mean-flow modifications $\nabla_{\overline{\mathsf{w}}}\lambda$. Since the eigenvalue is a function of the Jacobian, which is itself a function of the mean-flow, the eigenvalue is directly a function of the mean-flow. Therefore, a first-order Taylor

expansion leads to the following definition of $\nabla_{\overline{\mathsf{w}}}\lambda$:

$$\delta\lambda = \left\langle \nabla_{\overline{\mathsf{w}}}\lambda,\ \delta\overline{\mathsf{w}} \right\rangle, \tag{7}$$

where $\langle\rangle$ is a given scalar-product. The adjoint $\mathsf{J}^\dagger$ of the Jacobian J is defined such that, for any arbitrary vectors u and v we have $\langle \mathsf{u}, \mathsf{J}\mathsf{v}\rangle = \left\langle \mathsf{J}^\dagger\mathsf{u}, \mathsf{v}\right\rangle$. The adjoint modes $\check{\mathsf{w}}$ correspond to the solutions of the adjoint eigen-problem

$$\mathsf{J}^\dagger\check{\mathsf{w}} = \lambda^*\check{\mathsf{w}}, \tag{8}$$

where * designates the trans-conjugate of a complex quantity.

Finally, we can link the sensitivity gradient $\nabla_{\overline{\mathsf{w}}}\lambda$ to the direct $\hat{\mathsf{w}}$ and adjoint $\check{\mathsf{w}}$ modes with

$$\nabla_{\overline{\mathsf{w}}}\lambda = \mathsf{H}'^\dagger\check{\mathsf{w}}, \tag{9}$$

where $\mathsf{H}' = \partial[\mathsf{J}(\overline{\mathsf{w}})\hat{\mathsf{w}}]/\partial\overline{\mathsf{w}}$ is a linear operator related to the Hessian of the governing Navier-Stokes equations (the precise relation is given in the Appendix). The sensitivity of the frequency to mean-flow modifications is then given by the imaginary part of the gradient: $\nabla_{\overline{\mathsf{w}}}\omega = -\Im(\nabla_{\overline{\mathsf{w}}}\lambda)$. This vector-field highlights the sensitive regions of the flow, more precisely it indicates where and how to change the mean-flow to easily shift the frequency of the flow.

The mean-flow modification due to the introduction of a steady forcing is governed by

$$\mathcal{R}_f(\overline{\mathsf{w}} + \delta\overline{\mathsf{w}}) = \delta\mathsf{f}, \tag{10}$$

where $\mathcal{R}_f$ denotes the full RANS-equations closed with an appropriate turbulence-model. For small-amplitude forcings $\delta\mathsf{f}$, this equation may be linearized and the mean-flow modification obtained from: $\delta\overline{\mathsf{w}} \approx -\mathsf{J}_f^{-1}\delta\mathsf{f}$, where J_f is the Jacobian associated to $\mathcal{R}_f$. Here, we will evaluate two simplified approaches, which avoid the introduction of a turbulence model. The first consists in assuming that the eddy-viscosity is kept frozen and maintained equal to the eddy-viscosity associated to the unperturbed mean-flow $\overline{\mathsf{w}}$ as the external forcing $\delta\mathsf{f}$ is applied; this path will be followed in Sec. VII where we will indicate how to compute an eddy-viscosity $\overline{\mu}_t$ from an experiment or a numerical simulation. The second approach, which is more approximate, consists, on top of that, to assume that the eddy-viscosity is zero ($\overline{\mu}_t = 0$), i.e., the Jacobian J_f is replaced in the evaluation of the mean-flow modification by the laminar Jacobian J introduced in Eq. (6) and which is based solely on the molecular viscosity μ

$$\delta\overline{\mathsf{w}} \approx -\mathsf{J}^{-1}\delta\mathsf{f}. \tag{11}$$

Here, the symbol $\approx$ refers to the fact that this relation is a rough approximation. Introducing $\delta\overline{\mathsf{w}}$ from Eq. (11) into Eq. (7) then leads to the gradient of the eigenvalue with respect to the introduction of a steady forcing $\nabla_{\mathsf{f}}\lambda$

$$\delta\lambda = \left\langle \nabla_{\mathsf{f}}\lambda,\ \delta\mathsf{f} \right\rangle, \qquad \text{with} \qquad \nabla_{\mathsf{f}}\lambda = -\mathsf{J}^{\dagger-1}\nabla_{\overline{\mathsf{w}}}\lambda. \tag{12}$$

The sensitivity of the frequency to the introduction of a steady forcing may be obtained from: $\nabla_{\mathsf{f}}\omega = -\Im(\nabla_{\mathsf{f}}\lambda)$. This vector field indicates where to introduce a forcing that acts on the mean-flow to optimally modify the frequency of the flow.

III. NUMERICAL STRATEGY TO OBTAIN THE EIGENVALUE SPECTRUM AND THE SENSITIVITIES

The eigen-problems and the sensitivity gradients introduced above may be computed either within a continuous or a discrete framework. The continuous framework consists in deriving all partial differential equations defining the various quantities introduced above and then spatially discretize all equations. The partial differential equations defining the sensitivity gradients for the incompressible Navier-Stokes equations can be found in Marquet, Sipp, and Jacquin[8] and those related to the compressible Navier-Stokes equations in Meliga, Sipp, and Chomaz.[32] Various types of spatial discretizations may be used, such as finite elements[8] or finite differences.[33] In this study, we consider a discrete framework where the nonlinear Navier-Stokes equations are first discretized with a finite-volume technique and then linearized as proposed in Mettot, Renac, and Sipp.[12] Such

a procedure is numerically sound and precise, since first, the discretization choices are done only once, and second, the adjoint Jacobian is obtained up to machine precision since it is defined with the trans-conjugate of the Jacobian matrix.[12,34] In particular, we will show how a numerical code which time-marches the Navier-Stokes equations can be used in a black-box manner to extract the direct modes, adjoint modes, and various sensitivities.

We now illustrate this discrete strategy with the compressible Navier-Stokes equations, which after spatial discretization using finite volumes can be recast in the general following form:

$$\frac{d\mathsf{w}}{dt} = \mathcal{R}(\mathsf{w}). \tag{13}$$

Here, $\mathsf{w} \in \mathbb{R}^N$ represents the set of variables describing the flow at each spatial location of the mesh, for example, $(\rho, \rho\mathsf{u}, \rho E)$ if the density, momentum, and density times total energy are used to describe the flow. The operator $\mathcal{R} : \Omega \in \mathbb{R}^N \rightarrow \mathbb{R}^N$ is $\mathcal{C}^2$ over the domain Ω , and represents the discretized residual. Note that we assume here that it includes all boundary conditions. The size N of the vector w is equal to the product of the number of variable times the number of cells in the mesh.

A. Direct and adjoint eigenvalue problems

The Jacobian matrix J corresponds to the linearization of the discrete Navier-Stokes operator $\mathcal{R}$ around the mean-flow $\overline{\mathsf{w}}$, and verifies for an arbitrary vector u

$$\mathsf{J}\mathsf{u} = \frac{1}{\epsilon}\left[\mathcal{R}\left(\overline{\mathsf{w}} + \epsilon\mathsf{u}\right) - \mathcal{R}\left(\overline{\mathsf{w}}\right)\right]. \tag{14}$$

The parameter ϵ needs to be chosen carefully, since ϵ needs to be small enough to accurately approximate the Jacobian but not too small to avoid round-off errors.[35,36] We used double-precision arithmetics and chose values of ϵ that depend on the local value of the variable that is linearized: $\epsilon_i = \epsilon_m(|\overline{\mathsf{w}}_i| + 1)$ where $\overline{\mathsf{w}}_i$ is the ith component of the mean-flow vector and $\epsilon_m = 10^{-6}$ — we checked that same results were obtained with $\epsilon_m = 10^{-7}$. Then, by choosing a series of well-defined vectors u, we can compute all the Jacobian coefficients solely by residual evaluations, which are provided by the numerical code. Moreover, the Jacobian structure is intrinsically linked to the discretization stencil, which we chose to be compact, ensuring the sparsity of the matrix. The procedure is then optimized using a set of vectors u that takes into account the stencil discretization of the residual $\mathcal{R}$ as proposed by Mettot, Renac, and Sipp[12] in order to compute all the matrix J coefficients with only a few residual evaluations. Such numerical strategies also exist in common libraries such as PETSc,[37] where the explicit Jacobian is extracted from finite-difference evaluations with graph-coloring methods. Different strategies may then be used to solve the eigenvalue problem[34] in Eq. (6). Here, we focus on a shift-invert strategy (open source library ARPACK[38]) combined with a sparse direct LU parallel solver for matrices inversion (open source library MUMPS http://graal.ens-lyon.fr/MUMPS/). This procedure is computationally intensive in terms of memory but exploits the sparsity of the matrices and yields very fast and accurate results for two-dimensional problems (for three-dimensional configurations, an iterative solver would be better suited, see Mettot, Renac, and Sipp[12]).

In the following, for the definition of the adjoint mode $\check{\mathsf{w}}$, given in Eq. (8), we will use an inner product related to the discretization of the L2-function norm

$$\forall(\mathsf{u},\mathsf{v}) \qquad \langle \mathsf{u},\mathsf{v}\rangle = \sum_{i,j} u_i^* \Omega_{ij} v_j = \mathsf{u}^*\mathsf{Q}\mathsf{v}, \tag{15}$$

where Q is a positive-definite symmetric matrix. In the case of finite-volumes, Q is a diagonal matrix whose terms correspond to the volume of our mesh cells. The Jacobian being explicitly formed, we have direct access to the trans-conjugate of the Jacobian J^*. We may then straightforwardly compute the adjoint mode from $\check{\mathsf{w}} = \mathsf{Q}^{-1}\check{\mathsf{w}}_*$, where $\check{\mathsf{w}}_*$ is the eigenvector of J^* associated to the conjugate of λ

$$\mathsf{J}^*\check{\mathsf{w}}_* = \lambda^*\check{\mathsf{w}}_* \text{ with } \check{\mathsf{w}}_*^*\hat{\mathsf{w}} = 1. \tag{16}$$

B. Sensitivity gradients

After some derivation (see the Appendix and for more details Mettot, Renac, and Sipp[12]), we can show that the sensitivity gradient takes the form

$$\nabla_{\overline{\mathsf{w}}}\lambda = \mathsf{Q}^{-1}\mathsf{H}'^{*}\mathsf{Q}\check{\mathsf{w}}, \tag{17}$$

where the matrix H' is sparse and verifies for an arbitrary vector u

$$\mathsf{H}'\mathsf{u} = \frac{1}{\epsilon_1\epsilon_2}[\mathcal{R}\left(\overline{\mathsf{w}} + \epsilon_1\hat{\mathsf{w}} + \epsilon_2\mathsf{u}\right) - \mathcal{R}\left(\overline{\mathsf{w}} + \epsilon_1\hat{\mathsf{w}}\right) - \mathcal{R}\left(\overline{\mathsf{w}} + \epsilon_2\mathsf{u}\right) + \mathcal{R}\left(\overline{\mathsf{w}}\right)]. \tag{18}$$

Here, ϵ_1 and ϵ_2 are small parameters. The coefficients of H' may then be explicitly computed from residual evaluations using the previous equation. Note that the optimal set of vectors used for the Jacobian computation can also be used to compute the matrix H'.

The sensitivity of the eigenvalue with respect to the introduction of a steady forcing is finally obtained by computing

$$\nabla_{\mathsf{f}}\lambda = -\mathsf{Q}^{-1}\mathsf{J}^{*-1}\mathsf{Q}\nabla_{\overline{\mathsf{w}}}\lambda. \tag{19}$$

IV. UNSTEADY DYNAMICS

A. Configuration

We consider a D-shaped cylinder of height $D = 25$ mm, length $L = 2D$ and invariant in the z-direction. The computational domain consists in a section of width $W = 3D$ with periodic boundary conditions in the z-direction. On the inlet boundary, we impose a subsonic inflow condition characterized by the Mach number $M = 0.2$, the stagnation pressure $p_\infty = 11\,667$ Pa, and the stagnation temperature $T_\infty = 292.5$ K. The Reynolds number based on the cylinder height, the free stream density ρ_∞, velocity U_∞, and viscosity μ_∞ (computed with the Sutherland's law) is equal to $Re = 13\,000$. All quantities are made dimensionless using the cylinder height D and the free stream variables ρ_∞, U_∞, and T_∞, and the Strouhal number is defined with $S = fD/U_\infty$ where f is the dimensional frequency of the unsteadiness. This configuration mimics the studies led by Parezanović and Cadot[30] and Meliga, Pujals, and Serre.[29]

The mesh consists of two blocks discretized in the (x, y)-plane as depicted in Fig. 1(a), and uniformly extended in the third direction $0 \le z \le 3$ using a step $\Delta z = 7.7 \times 10^{-2}$. The computational border is taken at 20D from the cylinder center, which also corresponds to the origin of the cartesian coordinate system (x, y) (the cylinder base is located at $x = 1.5$). A tangential law for the evolution of the discretization steps Δx and Δy is used, imposing the cells adjacent to the downstream edge

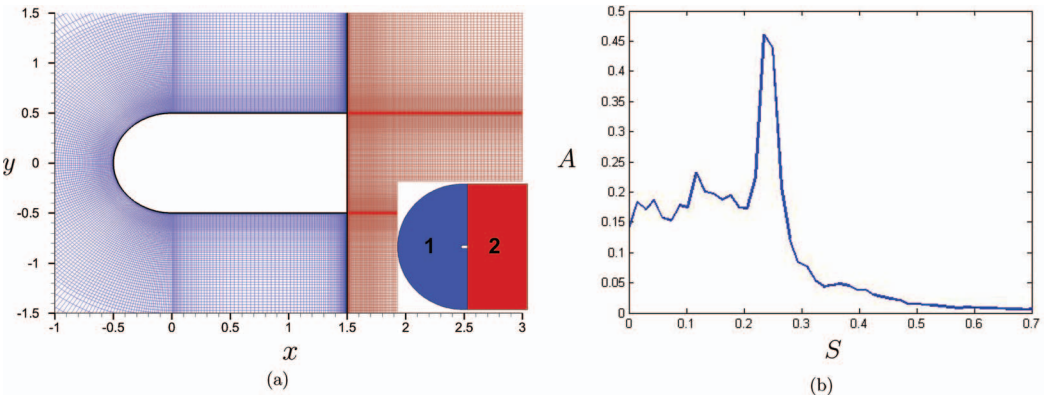

FIG. 1. (a) Mesh discretization near the cylinder. (b) Flow spectrum obtained with the signal extracted at a sensor located at $(x = 8, y = -0.5, z = 1.5)$.

TABLE I. Block discretization properties.

	Discretization points	Number of cells
Block 1	$357 \times 85 \times 40$	$30\,345 \times 40 = 1.2 \times 10^6$
Block 2	$150 \times 273 \times 40$	$40\,950 \times 40 = 1.6 \times 10^6$

of the cylinder to be square of size $\Delta x = 5 \times 10^{-4}$ as shown in Fig. 1(a). The mesh is slightly more refined in the separated region than in the reference study by Travin *et al.*[39] on circular cylinder flows. The blocks discretization properties are summarized in Table I and lead to a total number of cells of $N_m^{3D} = 2.85 \times 10^6$ for the unsteady 3D simulations and $N_m^{2D} = 71\,300$ for the 2D stability and sensitivity analyzes. Non-reflecting conditions are imposed on the outer parts of the domain, while a no-slip adiabatic condition is imposed on the cylinder surface.

B. 3D unsteady simulation

Rather than resolving all scales of the flow (as done in a DNS study), we use 3D unsteady RANS simulations to analyze the low-frequency dynamics of the flow. The small-scale turbulence is modeled using the SAS approach proposed by Menter and Egorov,[40] which includes an additional source term compared to the original $k - \omega$ SST model of Menter.[41] The effect of this source term is to reduce the eddy viscosity μ_t in areas where fluctuations are resolved, allowing the structures to stay alive and grow. Hence, this model differs from the classical turbulence models in the sense that it allows the resolution of a larger band of wavelength in the Kolmogorov spectrum. Note that the additional source term of the $k - \omega$ model has been slightly modified by imposing an upper-bound to the Karman length (SAS-αL model[42]). Benyoucef[42] have shown that the SAS-αL model accurately reproduces the unsteady features of the 3D wake behind a circular cylinder, which is a configuration close to our D-shaped one. Note however, that the focus of this article is not the SAS-αL model. We could have used any numerical (DNS, Large Eddy Simulation (LES), etc.) which provides an accurate mean-flow and a relevant low-frequency dynamics.

In the following, we use the same numerical code as Benyoucef,[42] the elsA software[43] developed at ONERA. It is a finite volume based code, the convective fluxes associated with the mean field and turbulent equations being discretized using the Roe scheme extended to the second order with a MUSCL method.[44] The Superbee limiter was applied to the mean field variables by default but it was checked that it had no influence on the solution — no shocks are present in the flow. Also, Harten's correction is used[45] and the Zheng limiter[46] (which is designed to limit the values of $\rho\omega$ outside the boundary layers) is activated. A central difference scheme is used for the turbulent diffusive fluxes. The viscous flux of the mean field is calculated at the interface by averaging cell-centered values of flux density, which are computed from cell-centered evaluation of gradients. The source terms are discretized using estimates of gradients and variables at cell centers.

C. Flow frequency and mean-flow computation

The time integration is performed using a second-order Gear method, based on a backward Euler scheme, with a global time step $\Delta t = 4.3 \times 10^{-4}$, which ensures that the CFL condition is below 1 in nearly all the computational domain (its value reaches a maximum value of 10 only in the first few cells close to the cylinder wall in the boundary layers, which is commonly accepted in such computations). We have recorded the time-evolution of the cross-stream velocity component 6.5 diameters downstream of the cylinder base at ($x = 8$, $y = -0.5$, $z = 1.5$). The spectrum is obtained by determining the PSD (Welch method) of this signal, see Fig. 1(b).

We observe a strong peak at a Strouhal number of $S = 0.23$ in close agreement with the one measured experimentally, $S = 0.22$.[30] We have depicted in Fig. 2 the Q-criterion contours of a typical snapshot of the flow-field once the oscillatory regime is reached. We observe that, as in the experiment, separation occurs on the lower and upper walls of the cylinder, and that the flow exhibits

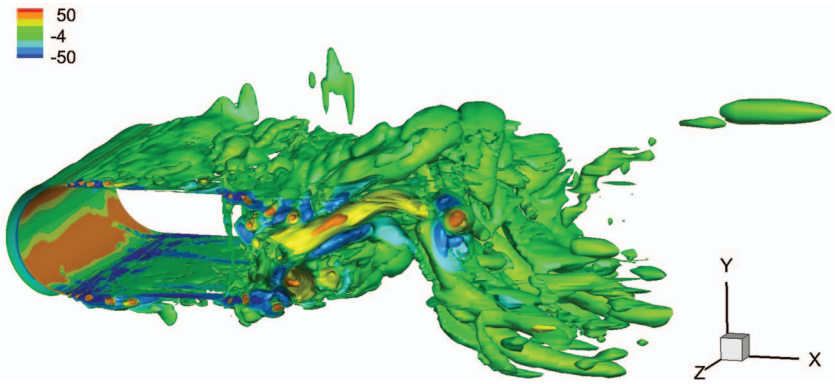

FIG. 2. Q-criterion contours of the flow field at an arbitrary time in the oscillating regime.

structures typical of a Von-Kármán street in the wake of the object. Yet, we can see that the flow is fully three-dimensional, as expected from the SAS-αL model.

The mean-flow $\overline{\mathsf{w}}(x, y)$ is then computed by averaging the unsteady snapshots both in time and in the z-direction. Contours of the stream-wise velocity ρu are plotted in Fig. 3(a) together with the streamlines of the mean-flow. We observe a recirculation bubble at the rear part of the cylinder of length $\overline{l_r} = 0.89$, in relative agreement (8.5% error) with the experimental result $\overline{l_r} = 0.82$ of Parezanović and Cadot[30] (note that the mean-flow obtained from 2D Spalart-Allmaras simulations exhibits a recirculation length $\overline{l_r} = 0.56$, that is 30% lower than the experimental value[29]).

V. DIRECT AND ADJOINT MODES

The linear stability analysis is performed as presented in Sec. III using a fully discrete formalism. As explained in Sec. III, to extract the Jacobian and the matrix H' of the governing equations $\mathcal{R}$, we need to select a spatial discretization which ensures that $\mathcal{R}$ is $\mathcal{C}^2$. In the following, we have therefore switched off the Superbee limiter in the elsA code.

We here restrict the analysis to two-dimensional perturbations, which are the most unstable. This can be understood from Squire's theorem,[47] which ensures that Kelvin-Helmholtz instabilities are strongest for such perturbations. The size of the Jacobian matrix J is equal to the number of cells $N_m^{2D} = 71\,300$ times the number of variables, here 4 (ρ, ρu, ρv, ρE), i.e., 285 000 number of degrees of freedom in the direct and adjoint eigenmodes. The Jacobian matrix J is extracted and its spectrum is analyzed in Fig. 3(b). Similar to Meliga, Pujals, and Serre,[29] we observe the existence of a slightly unstable eigen-mode with a Strouhal number $S = 0.26$ close to the value computed from the unsteady simulations ($S = 0.23$) and in good agreement with the experiment from Parezanović

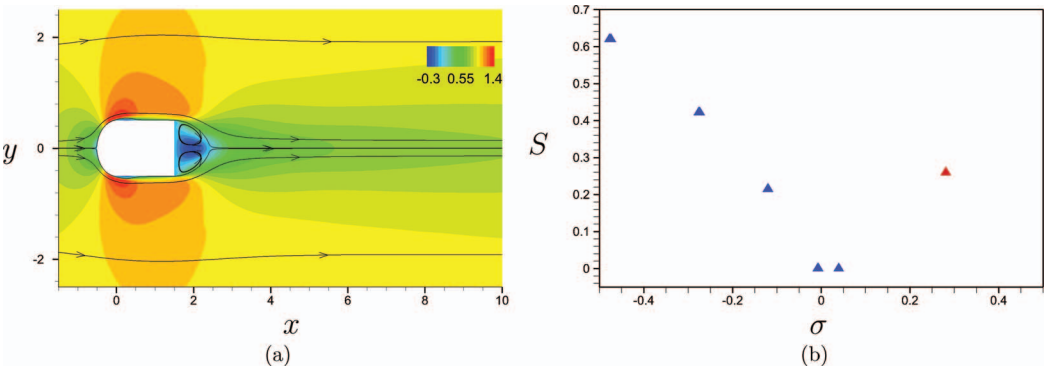

FIG. 3. (a) Stream-wise velocity contours ρu and streamlines of the 2D mean-flow $\overline{\mathsf{w}}(x, y)$. (b) Stability spectrum of the mean-flow for 2D perturbations in the amplification rate-Strouhal number plane.

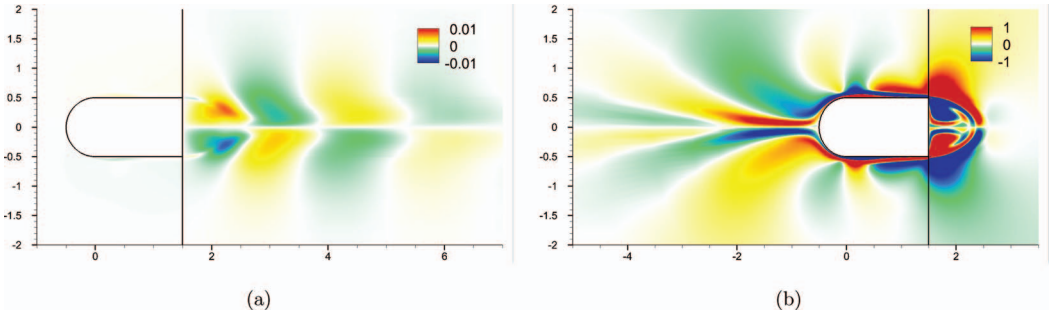

FIG. 4. Spatial structure of the stream-wise momentum component ρu of (a) the direct unstable mode $\hat{\mathbf{w}}$ and (b) the adjoint unstable mode $\check{\mathbf{w}}$, using only a molecular viscosity for the definition of the Jacobian. Only the real part is depicted. The vertical solid lines are visualization artefact due to the presence of 2 blocks.

and Cadot[30] ($S = 0.22$) and the numerical results of Meliga, Pujals, and Serre[29] ($S = 0.23$ for the 2D unsteady RANS simulations and $S = 0.25$ for the stability analysis with the linearized RANS model). As a consequence, a laminar model yields a good first order prediction of the unstable mode frequency. The spatial structure of the direct mode $\hat{\mathbf{w}}$ is depicted in Fig. 4(a), while the corresponding adjoint mode structure $\check{\mathbf{w}}$ is shown Fig. 4(b). Note that both modes include 4 components, one for each conservative variable ρ, ρu, ρv, and ρE; here, we only depicted the stream-wise component.

We recover typical structures of Kelvin-Helmholtz instabilities with an opposite traveling direction between the direct and adjoint modes. This feature is due to the opposite sign in the convective part of the direct and adjoint equations responsible for the non-normality of the Jacobian.[48] Both direct and adjoint mode structures compare well to those computed in Meliga, Pujals, and Serre.[29]

The following comments can be made regarding the spatial convergence and robustness of the eigenvalues/eigenvectors. We note that the 2D mean-flow is smoother than any flow snapshot captured by the 3D simulation (because the mean-flow is the result of an averaging process). Hence, the 2D mesh (which is a slice of the 3D mesh) is sufficiently refined to well represent all features that appear in the 3D snapshots and therefore in the 2D mean-flow (shear-layers, boundary-layers). Finally note that, in stability analyzes, the convergence issues are most often seen on the amplification rate while the frequency is usually a more robust quantity. Since the quasi-laminar stability and sensitivity analyzes focus on this latter quantity, we are confident in the fact that the present results display good convergence and robustness properties.

VI. PASSIVE CONTROL

A. Sensitivity gradients

The matrix H' is then extracted and the sensitivity gradient to mean-flow perturbations $\nabla_{\overline{\mathbf{w}}}\lambda$ computed. We will focus only in the following on the sensitivity of the frequency $\nabla_{\overline{\mathbf{w}}}\omega$, since the amplification rate is not physically relevant in the case of mean-flow stability analyzes.

We plotted in Fig. 5(a) the spatial structure of the frequency sensitivity $\nabla_{\overline{\mathbf{w}}}\omega$. The flow is mostly sensitive near the cylinder surface and inside the recirculation bubble.

The frequency sensitivity to a steady force $\nabla_{\mathbf{f}}\omega$ is then computed and depicted in Fig. 5(b). We observe that a steady force in the stream-wise direction will induce an increase of the mode frequency near the cylinder surface ($x < 1.5$ in the figure), while a similar tendency can be observed in most part of the recirculating area.

B. Steady control of the flow frequency

Similar to Meliga, Pujals, and Serre,[29] we consider the impact of a control cylinder of diameter $d = 0.04D$ onto the flow frequency. The force exerted on the mean-flow by a cylinder of diameter d, located at (x_c, y_c) where the velocity and density of the mean-flow are equal to $\overline{\mathbf{u}}(x_c, y_c)$ and $\overline{\rho}(x_c, y_c)$

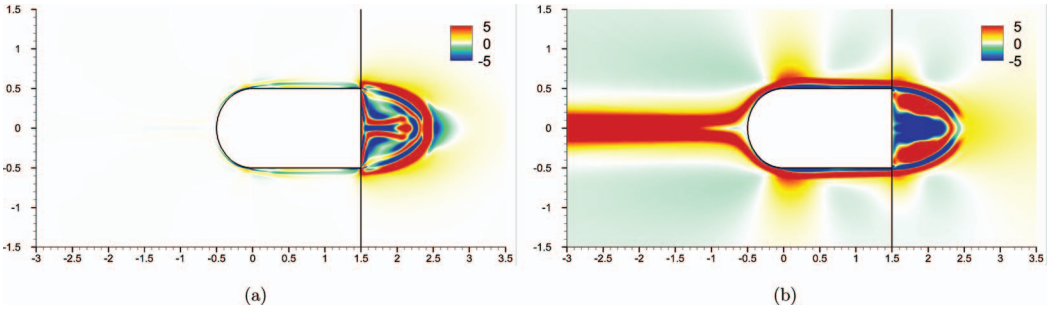

FIG. 5. Spatial structure of the stream-wise momentum component ρu of (a) the frequency sensitivity to mean-flow perturbations $\nabla_{\overline{\mathsf{w}}}\omega$, and (b) the frequency sensitivity to a steady force $\nabla_{\mathsf{f}}\omega$. The real part is plotted.

may be approximated by the following expression:[8]

$$\mathsf{f}_{(x_c,y_c)}(x,y) = -\frac{1}{2} d C_d \overline{\rho}\overline{\mathsf{u}} \left\|\overline{\mathsf{u}}\right\| \delta(x-x_c, y-y_c), \tag{20}$$

where $\delta(x-x_c, y-y_c)$ refers to the Kronecker symbol at (x_c, y_c), indicating that the force is applied on an infinitely small spatial support. Note that for the numerical treatment, $\delta(x-x_c, y-y_c)$ is approximated by a field equal to zero in all cells of the mesh, except at the cell located at (x_c, y_c), where it is set to the inverse of the cell area. The drag coefficient was chosen to be equal to $C_d = 1$, which is approximately valid for a circular cylinder flow characterized by Reynolds numbers ranging from 10^2 to 10^5. In the experiment of Parezanović and Cadot,[30] the Reynolds number based on the free-stream velocity and the control cylinder radius is equal to 520 in the experiment, which justifies the chosen value of C_d. The control maps $\delta\omega_{(x_c,y_c)} = \left\langle \nabla_{\mathsf{f}}\omega, \mathsf{f}_{(\mathsf{x_c},\mathsf{y_c})} \right\rangle$, which indicate the variation of the frequency of the unstable global mode due to the presence of the control cylinder at (x_c, y_c), are shown in the upper part of Fig. 6(a) and can be compared to the previous results of Meliga, Pujals, and Serre[29] in the upper part of Fig. 6(b) and to those of the experiment by Parezanović and Cadot[30] in the lower parts of each figure. We can see that the results obtained with the quasi-laminar stability/sensitivity approach yield results that are quantitatively similar to those of the experiment of Parezanović and Cadot[30] and to those obtained with a linearized RANS model closed with a Spalart-Allmaras model (Fig. 6(b)).[29] These results are very interesting from an industrial application point of view. Indeed, they suggest that the impact of a steady device on the frequency spectrum of the flow can be approximated using a simple laminar model in a linear stability analysis applied to the mean-flow. We therefore avoid the inherent complexity of a turbulence model or the definition of an eddy viscosity.

Note finally that we did not take into account the influence of the cylinder flow at the perturbation level, as introduced by Hill,[5] Marquet *et al.*,[49] Meliga, Sipp, and Chomaz,[32] Pralits, Brandt, and Giannetti,[33] and Meliga, Pujals, and Serre,[29] since it was shown in these references that this term was always at least one order of magnitude smaller than the term related to the base-flow perturbations.

VII. ACCURATE EVALUATION OF THE EFFECT OF THE CONTROL CYLINDER ON THE MEAN-FLOW

We have estimated in Sec. VI the impact of a steady force on the mean-flow with Eq. (11), which is based on a Jacobian J defined solely with the molecular viscosity. As discussed in Sec. II, we know that this is a very gross approximation since the mean-flow is not governed with laminar equations but with equations involving Reynolds stresses. Hence, to improve the results, we now evaluate the mean-flow modification $\delta\overline{\mathsf{w}}$ by a frozen-eddy viscosity approach: $\delta\overline{\mathsf{w}} \approx -\mathsf{J}_{\overline{\mu}_t}^{-1}\delta\mathsf{f}$, where $\mathsf{J}_{\overline{\mu}_t}$ is the Jacobian based on an added eddy-viscosity. Instead of Eqs. (12) and (19), we are led to the following expression of the eigenvalue sensitivity to the introduction of a steady forcing:

$$\nabla_{\mathsf{f}}\lambda = -\mathsf{J}_{\overline{\mu}_t}^{\dagger -1}\nabla_{\overline{\mathsf{w}}}\lambda = -\mathsf{Q}^{-1}\mathsf{J}_{\overline{\mu}_t}^{* -1}\mathsf{Q}\nabla_{\overline{\mathsf{w}}}\lambda, \tag{21}$$

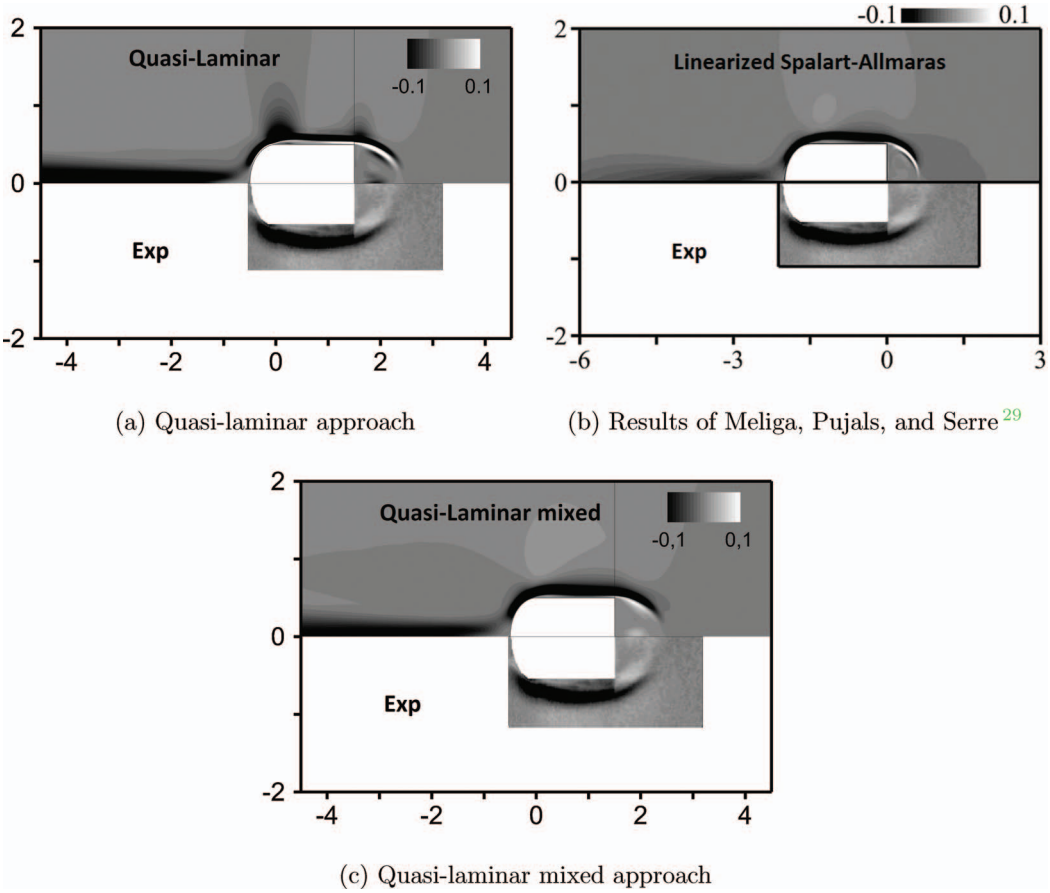

(a) Quasi-laminar approach

(b) Results of Meliga, Pujals, and Serre [29]

(c) Quasi-laminar mixed approach

FIG. 6. Frequency variation $\delta\omega_{(x_c,y_c)}$ of the flow due to the presence of a small control cylinder located at (x_c, y_c). The results of the quasi-laminar stability/sensitivity analyzes are reported in upper part of Figure (a), while those obtained with a linearized RANS model involving a Spalart-Allmaras turbulence model[29] are given in the upper part of Figure (b). In the upper part of Figure (c), we have plotted the results given by a quasi-laminar mixed approach, in which an eddy-viscosity has been taken into account for the evaluation of the mean-flow modifications due to the introduction of a steady forcing (see Sec. VIII). In all figures, the lower part of the plot depicts the experimental results from Parezanović and Cadot[30] and which were taken from Meliga, Pujals, and Serre.[29] Reproduced with permission from P. Meliga, G. Pujals, and E. Serre, Phys. Fluids **24**, 061701 (2012). Copyright 2012 AIP Publishing LLC.

where $\nabla_{\overline{\mathsf{w}}}\lambda$ remains unchanged and designates the sensitivity of the eigenvalue to mean-flow modifications defined in Eqs. (9) and (17). This approach will be called quasi-laminar mixed approach in the following.

This naturally raises the question of the determination of an eddy viscosity $\overline{\mu}_t$ from numerical results or experimental data. For a homogeneous incompressible flow with density ρ, a simple approach to define the eddy viscosity $\overline{\mu}_t$ consists in first computing the mean velocity $\overline{u_i}$, as well as the Reynolds stress tensor $\overline{u_i'u_j'}$ from the experimental or DNS data-sets. In the following, we will use the standard Reynolds decomposition $\mathsf{w} = \overline{\mathsf{w}} + \mathsf{w}'$, in which the fluctuating component w' incorporates both the organized wave and the turbulent motions. The production of turbulent kinetic energy $\overline{P}$ can then be computed from

$$\overline{P} = -\rho\overline{u_i'u_j'}\partial_j\overline{u_i}, \tag{22}$$

while the Boussinesq relation reads

$$\rho\overline{u_i'u_j'} = \frac{2}{3}\rho\overline{k}\delta_{ij} - 2\overline{\mu}_t\overline{S}_{ij}. \tag{23}$$

Multiplying this relation by $\partial_j \overline{u}_i$ and summing over all indices finally yields

$$\overline{\mu}_t = \frac{\overline{P}}{2\overline{S}_{ij}\overline{S}_{ij}}. \tag{24}$$

We will not follow this general idea here, but rather take advantage of the fact that the mean-flow has been determined in this study by time-averaging a SAS $k-\omega$ model. Winckelmans, Jeanmart, and Carati[50] showed that the Reynolds stress tensor (required for the evaluation of $\overline{P}$) actually corresponds to the sum of a resolved part — which yields a resolved part of the eddy-viscosity shown in Eq. (24) — and a modeled part — which induces a modeled part of the eddy-viscosity, given by the time-averaged turbulent variables $\overline{\mu}_t = \rho\overline{k}/\overline{\omega}$. We propose in a first approximation to consider only the modeled part. We believe that this approximation is sufficient here since the region where the flow is most sensitive — near the cylinder surface ($x < 1.5$) — also corresponds to a region where the unsteadiness in the resolved part is reasonably weak. The frequency control map of the quasi-laminar mixed approach — Eq. (21) — based on the modeled eddy-viscosity, is shown in the upper part of Fig. 6(c). We can see that the plot is smoother and even closer to the experimental result of Parezanović and Cadot[30] (lower part of the figure).

VIII. CONCLUDING REMARKS

We performed in this study a linear stability analysis of a turbulent mean-flow, where a quasi-laminar model was used to compute the eigen-modes and sensitivities of the flow. In particular, we found that such a simple approach recovers quantitatively the frequency shifts observed in the experimental work by Parezanović and Cadot.[30] The present quasi-laminar approach is very general and may be applied as soon as a mean-flow is available. Such a mean-flow may be obtained either by numerical means (DNS, LES, unsteady RANS simulation, steady RANS simulations) or experimental measurements.

With respect to the work of Meliga, Pujals, and Serre,[29] the present results give new physical insight for shifting the low-frequency of a turbulent flow: it is suggested that accurately capturing the mean-flow is most important and that the low-frequency of a turbulent flow is best captured by a quasi-laminar stability analysis. This indicates that the Spalart-Allmaras model used in Meliga, Pujals, and Serre[29] plays a negligible role in the prediction of the sensitive regions of the flow. Having identified the key-enablers for this prediction, i.e., an accurate mean-flow and a quasi-laminar sensitivity analysis, now opens the opportunity to tackle a wider range of flow configurations — all turbulent flows driven by Kelvin-Helmholtz type instabilities — and a wider range of situations — both numerical and experimental mean-flows may come as an input to the present analysis. We have also shown how to construct an eddy-viscosity field from a series of velocity snapshots if the more precise quasi-laminar mixed approach is required.

Note finally that the velocity field is sufficient to describe the flow physics in the case of uniform density flows driven by incompressible Navier-Stokes equations, while also the density and the temperature fields are required in the compressible case. With Particle Image Velocimtery (PIV) measurements in an experiment, it is easy to extract velocity mean-flows. In the compressible case, a first approximate of the density and temperature fields may be obtained by assuming that the stagnation temperature and the stagnation pressure are constant in the whole domain (which is a gross approximation, especially for the stagnation pressure in viscous layers).

APPENDIX: DERIVATION OF THE SENSITIVITY GRADIENT OF THE EIGENVALUE TO MEAN-FLOW MODIFICATIONS

We detail here the derivation of the sensitivity gradient of the eigen-value to mean-flow modifications $\nabla_{\overline{\mathbf{w}}}\lambda$ in a discrete framework. Considering a small mean-flow variation $\delta\overline{\mathbf{w}}$, the eigenvalue problem in Eq. (6) is perturbed and becomes to the first order

$$\boldsymbol{\delta}\mathbf{J}\hat{\mathbf{w}} + \mathbf{J}\delta\hat{\mathbf{w}} = \delta\lambda\hat{\mathbf{w}} + \lambda\delta\hat{\mathbf{w}}. \tag{A1}$$

We then multiply the previous equation with the trans-conjugate of the adjoint vector $\check{\mathsf{w}}_*^*$, defined in Eq. (16)

$$\delta\lambda = \check{\mathsf{w}}_*^* \boldsymbol{\delta}\mathsf{J}\hat{\mathsf{w}}. \tag{A2}$$

If $\boldsymbol{\delta}\mathsf{J}$ corresponds to a variation of the Jacobian induced by a variation of the mean-flow $\delta\overline{\mathsf{w}}$, then

$$\boldsymbol{\delta}\mathsf{J}\hat{\mathsf{w}} = \left.\frac{\partial(\mathsf{J}\hat{\mathsf{w}})}{\partial \mathsf{w}}\right|_{\mathsf{w}=\overline{\mathsf{w}}} \boldsymbol{\delta}\overline{\mathsf{w}}, \tag{A3}$$

where the global mode $\hat{\mathsf{w}}$ is assumed to be frozen. This expression may be written in a different manner using the Hessian H of $\mathcal{R}$

$$\boldsymbol{\delta}\mathsf{J}\hat{\mathsf{w}} = \mathsf{H}(\hat{\mathsf{w}}, \delta\overline{\mathsf{w}}). \tag{A4}$$

Here, $\mathsf{H}(\mathsf{u}, \mathsf{v})$ designates the vector z such that $\mathsf{z}_i = \sum_{j,k} \mathsf{H}_{ijk}\mathsf{u}_j\mathsf{v}_k$, with

$$\mathsf{H}_{ijk} = \left.\frac{\partial^2 \mathcal{R}_i}{\partial \mathsf{w}_j \partial \mathsf{w}_k}\right|_{\mathsf{w}=\overline{\mathsf{w}}}. \tag{A5}$$

Let us introduce the matrix H' such that $\mathsf{H}'\delta\overline{\mathsf{w}} = \mathsf{H}(\hat{\mathsf{w}}, \delta\overline{\mathsf{w}})$ for all $\delta\overline{\mathsf{w}}$. Equation (A4) may then be rewritten as

$$\boldsymbol{\delta}\mathsf{J}\hat{\mathsf{w}} = \mathsf{H}'\delta\overline{\mathsf{w}}. \tag{A6}$$

Introducing Eq. (A6) into (A2), we have

$$\delta\lambda = \check{\mathsf{w}}_*^*\mathsf{H}'\delta\overline{\mathsf{w}} = \langle \mathsf{Q}^{-1}\mathsf{H}'^*\mathsf{Q}\check{\mathsf{w}}, \delta\overline{\mathsf{w}}\rangle. \tag{A7}$$

The sensitivity gradient $\nabla_{\overline{\mathsf{w}}}\lambda$ verifies by definition (7) so that by identification we obtain the following expression of the gradient:

$$\nabla_{\overline{\mathsf{w}}}\lambda = \mathsf{Q}^{-1}\mathsf{H}'^*\mathsf{Q}\check{\mathsf{w}}. \tag{A8}$$

[1] S. Collis, R. Joslin, A. Seifert, and V. Theofilis, "Issues in active flow control: Theory, control, simulation, and experiment," Prog. Aerosp. Sci. **40**, 237–289 (2004).
[2] J.-M. Chomaz, "Global instabilities in spatially developing flows: Non-normality and nonlinearity," Annu. Rev. Fluid Mech. **37**, 357 (2005).
[3] J. Kim and T. R. Bewley, "A linear systems approach to flow control," Annu. Rev. Fluid Mech. **39**, 383–417 (2007).
[4] D. Sipp, O. Marquet, O. Meliga, and A. Barbagallo, "Dynamics and control of global instabilities in open flows: A linearized approach," Appl. Mech. Rev. **63**, 030801 (2010).
[5] D. C. Hill, "A theoretical approach for analyzing the restabilization of wakes," AIAA Paper No. 92-0067, 1992.
[6] A. Dobrinsky and S. Collis, "Adjoint parabolized stability equations for receptivity prediction," AIAA Paper 2000-2651, 2000.
[7] A. Bottaro, P. Corbett, and P. Luchini, "The effect of base flow variation on flow stability," J. Fluid Mech. **476**, 293–302 (2003).
[8] O. Marquet, D. Sipp, and L. Jacquin, "Sensitivity analysis and passive control of cylinder flow," J. Fluid Mech. **615**, 221–252 (2008).
[9] P. J. Strykowski and K. R. Sreenivasan, "On the formation and suppression of vortex shedding at low Reynolds-numbers," J. Fluid Mech. **218**, 71–107 (1990).
[10] W. Reynolds and A. Hussain, "The mechanics of an organized wave in turbulent shear flow. Part 3. Theoretical models and comparisons with experiments," J. Fluid Mech. **54**, 263–288 (1972).
[11] J. D. Crouch, A. Garbaruk, and D. Magidov, "Predicting the onset of flow unsteadiness based on global instability," J. Comput. Phys. **224**, 924–940 (2007).
[12] C. Mettot, F. Renac, and D. Sipp, "Computation of eigenvalue sensitivity to base flow modifications in a discrete framework: Application to open-loop control," J. Comput. Phys. **269**, 234–258 (2014).
[13] D. Sipp and A. Lebedev, "Global stability of base and mean flows: A general approach and its applications to cylinder and open cavity flows," J. Fluid Mech. **593**, 333–358 (2007).
[14] M. Shur, P. R. Spalart, K. D. Squires, M. Strelets, and A. Travin, "Three dimensionality in Reynolds-averaged Navier-Stokes solutions around two-dimensional geometries," AIAA J. **43**, 1230–1242 (2005).
[15] P. R. Spalart, "Detached-eddy simulation," Annu. Rev. Fluid Mech. **41**, 181–202 (2009).
[16] C. Juan and J. Jiménez, "Linear energy amplification in turbulent channels," J. Fluid Mech. **559**, 205–213 (2006).
[17] C. Cossu, G. Pujals, and S. Depardon, "Optimal transient growth and very large-scale structures in turbulent boundary layers," J. Fluid Mech. **619**, 79 (2009).

[18] E. Piot, G. Casalis, F. Muller, and C. Bailly, "Investigation of the PSE approach for subsonic and supersonic hot jets: Detailed comparisons with LES and linearized Euler equations results," Int. J. Aeroacoust. **5**, 361–393 (2006).
[19] T. Suzuki and T. Colonius, "Instability waves in a subsonic round jet detected using a near-field phased microphone array," J. Fluid Mech. **565**, 197–226 (2006).
[20] K. Gudmundsson and T. Colonius, "Instability wave models for the near-field fluctuations of turbulent jets," J. Fluid Mech. **689**, 97–128 (2011).
[21] G. E. Mattingly and W. O. Criminale, "The stability of an incompressible two-dimensional wake," J. Fluid Mech. **51**, 233–272 (1972).
[22] G. S. Triantafyllou, M. S. Triantafyllou, and C. Chryssostomidis, "On the formation of vortex streets behind stationary cylinders," J. Fluid Mech. **170**, 461–477 (1986).
[23] B. Pier, "On the frequency selection of finite-amplitude vortex shedding in the cylinder wake," J. Fluid Mech. **458**, 407–417 (2002).
[24] B. Thiria and J. E. Wesfreid, "Stability properties of forced wakes," J. Fluid Mech. **579**, 137–161 (2007).
[25] D. A. Hammond and L. G. Redekopp, "Global dynamics of symmetric and asymmetric wakes," J. Fluid Mech. **331**, 231–260 (1997).
[26] D. Barkley, "Linear analysis of the cylinder wake mean flow," EPL **75**, 750 (2006).
[27] M. Juniper, "Absolute and convective instability in gas turbine fuel injectors," in *Proceedings of the ASME Turbo Expo 2012: Power for Land, Sea and Air, Copenhagen, 2012* (ASME, New York, 2012).
[28] W. V. R. Malkus, "Outline of a theory of turbulent shear flow," J. Fluid Mech. **1**, 521–539 (1956).
[29] P. Meliga, G. Pujals, and E. Serre, "Sensitivity of 2-D turbulent flow past a D-shaped cylinder using global stability," Phys. Fluids **24**, 061701 (2012).
[30] V. Parezanović and O. Cadot, "Experimental sensitivity analysis of the global properties of a two-dimensional turbulent wake," J. Fluid Mech. **693**, 115–149 (2012).
[31] R. Mittal and S. Balachandar, "Effect of three-dimensionality on the lift and drag of nominally two-dimensional cylinders," Phys. Fluids **7**, 1841–1865 (1995).
[32] P. Meliga, D. Sipp, and J.-M. Chomaz, "Open-loop control of compressible afterbody flows using adjoint methods," Phys. Fluids **22**, 054109 (2010).
[33] J. Pralits, L. Brandt, and F. Giannetti, "Instability and sensitivity of the flow around a rotating circular cylinder," J. Fluid Mech. **650**, 513 (2010).
[34] M. F. de Pando, D. Sipp, and P. Schmid, "Efficient evaluation of the direct and adjoint linearized dynamics from compressible flow solvers," J. Comput. Phys. **231**, 7739–7755 (2012).
[35] D. Knoll and D. Keyes, "Jacobian-free Newton–Krylov methods: A survey of approaches and applications," J. Comput. Phys. **193**, 357–397 (2004).
[36] C. J. Mack and P. J. Schmid, "Direct numerical study of hypersonic flow about a swept parabolic body," Comput. Fluids **39**, 1932–1943 (2010).
[37] S. Balay, M. F. Adams, J. Brown, P. Brune, K. Buschelman, V. Eijkhout, W. D. Gropp, D. Kaushik, M. G. Knepley, L. C. McInnes, K. Rupp, B. F. Smith, and H. Zhang, "PETSc users manual," Technical Report No. ANL-95/11, Revision 3.4 (Argonne National Laboratory, 2013).
[38] R. Lehoucq, D. Sorensen, and C. Yang, *ARPACK Users' Guide: Solution of Large-scale Eigenvalue Problems with Implicitly Restarted Arnoldi Methods* (SIAM, 1998), Vol. 6.
[39] A. Travin, M. Shur, M. Strelets, and P. Spalart, "Detached-eddy simulations past a circular cylinder," Flow, Turbul. Combust. **63**, 293–313 (1999).
[40] F. Menter and Y. Egorov, "The scale-adaptive simulation method for unsteady turbulent flow predictions. Part 1: Theory and model description," Flow, Turbul. Combust. **85**, 113–138 (2010).
[41] F. Menter, "Two-equation eddy-viscosity turbulence models for engineering applications," AIAA J. **32**, 1598–1605 (1994).
[42] F. Benyoucef, "Amélioration de la prévision des écoulements turbulent par une approche URANS avancée," Thèse de l'Institut Supérieur de l'Aéronautique et de l'Espace, 2012.
[43] L. Cambier, S. Heib, and S. Plot, "The Onera elsA CFD software: Input from research and feedback from industry," Mech. Ind. **14**, 159–174 (2013).
[44] B. Van Leer, "Towards the ultimate conservative difference scheme. V. A second-order sequel to Godunov's method," J. Comput. Phys. **32**, 101–136 (1979).
[45] A. Harten and H. Hyman, "Self adjusting grid methods for one-dimensional hyperbolic conservation laws," J. Comput. Phys. **50**, 235–269 (1983).
[46] X. Zheng, C. H. Sung, T. T. Huang, C. Lia, and C. Liu, "Multigrid computation of incompressible flows using two-equation turbulence models: Part I—Numerical method," J. Fluids Eng. **119**, 893–899 (1997).
[47] P. Drazin and W. Reid, *Hydrodynamic Stability*, Cambridge Mathematical Library (Cambridge University Press, 2004).
[48] O. Marquet, M. Lombardi, J.-M. Chomaz, D. Sipp, and L. Jacquin, "Direct and adjoint global modes of a recirculation bubble: Lift-up and convective non-normalities," J. Fluid Mech. **622**, 1–21 (2009).
[49] O. Marquet, D. Sipp, L. Jacquin, and J.-M. Chomaz, "Multiple timescale and sensitivity analysis for the passive control of the cylinder flow," AIAA Paper 2008-4228, 2008.
[50] G. Winckelmans, H. Jeanmart, and D. Carati, "On the comparison of turbulence intensities from large-eddy simulation with those from experiment or direct numerical simulation," Phys. Fluids **14**, 1809 (2002).